AIMS Energy, 13(3): 732–755.
DOI: 10.3934/energy.2025026
Received: 09 March 2025
Revised: 05 June 2025
Accepted: 24 June 2025
Published: 27 June 2025

https://www.aimspress.com/journal/energy

Research article

Enhancing efficiency in TiO_2/$MAPbI_3$/GO perovskite solar cells: theoretical investigation of $MAPbI_3$ interlayer effects using SCAPS-1D simulation

Hmoud Al Dmour[1,*], Osama Y. Al-Madanat[2,*], Rakan M. Altarawneh[2], Emad K. Jaradat[3], Beddiaf Zaidi[4] and Bonginkosi V Kheswa[5]

[1] Department of Physics, Faculty of Science, Mutah University, 6170 Mutah, Jordan
[2] Department of Chemistry, Faculty of Science, Mutah University, 6170 Mutah, Jordan
[3] Department of Physics, Faculty of Science. Imam Mohammad Ibn Saud Islamic University, Riyadh 11623, Saudi Arabia
[4] Department of Physics, Faculty of Material Sciences, University of Batna 1, Batna, Algeria
[5] Department of Physics, University of Johannesburg, 55 Beit Street, Johannesburg, 2028, South Africa

* **Correspondence:** Email: hmoud79@mutah.edu.jo, madanat@mutah.edu.jo; Tel: +96232372380.

Abstract: Pursuing highly stable and efficient renewable energy solutions remains the driving force for developing perovskite solar cells (PSCs). Central to achieving these cells' high and optimum performance is the accurate and intelligent design engineering of the device's architecture. This theoretical study employs the simulation platform SCAPS-1D to systematically investigate the crucial role of the interlayer methylammonium lead iodide ($MAPbI_3$) as an adsorber layer in encouraging the titanium dioxide (TiO_2)/$MAPbI_3$/graphene oxide (GO) heterostructure design. By strategic tuning of the $MAPbI_3$ absorber layer, we successfully delivered a remarkable 20.8% power conversion efficiency (PCE) and fill factor (FF) of 80.5% at 300 K, significant improvements over the reference PCE of 11.6% and FF of 78.5%. Significant improvements were made by optimizing $MAPbI_3$ thickness to 1.2 μm and narrowing its bandgap to 1.5 eV, allowing enhanced photon absorption and charge carrier separation and minimizing interface-mediated recombination losses. Importantly, changes to the TiO_2 and GO layer thickness had a minimal impact on performance, emphasizing the absorber layer's dominant role in controlling efficiency. Utilizing low-cost, low-toxicity materials such as abundant TiO_2 and GO improves economic feasibility and scalability, and the optimized structure

minimizes material consumption, all aligning with sustainable photovoltaic development. These results advance our understanding of PSC optimization and reflect the enormous potential of $MAPbI_3$ materials for developing highly efficient, green alternatives to conventional solar technology, enabling future developments in stable, scalable, and environmentally friendly energy solutions.

Keywords: solar cells; open circuit voltage; multiple junctions; SCAPS-1D simulation

1. Introduction

Further progress in low-cost energy-conversion technologies is of key importance for meeting the world's needs for energy and combating climate change [1]. One of the main reasons for the significance of renewable energy sources is their potential as an alternative to fossil fuels in the face of climate change and environmental pollution [2]. It has been established that global warming and climate change are caused by greenhouse gas emissions from burning fossil fuels, and renewable energy can help reduce such emissions. Solar energy is considered one of the most promising alternatives because of its environmentally friendly nature and global availability [3,4]. For this reason, the development and deployment of renewable energy technologies tend to have higher up-front costs in the short run than non-renewable energy sources do. However, renewable energy is usually cheaper in the long term because fuel does not have to be regularly bought, and the cost is likely to come down with technological improvements and the realization of economies of scale [1,5,6]. Out of several sources of energy available under renewable sources, solar energy happens to be the most promising one and the most applicable renewable energy technology. It utilizes photovoltaic panels to convert sunlight into electrical power. Solar energy is clean, widely available, and provides for utilization in many applications, including the generation of electricity, heating, and lighting, due to its relative ease of installation and maintenance. There are different types of solar cells, such as traditional inorganic crystalline silicon cells, organic cells made up of polymers or small molecules, and organic-inorganic hybrid solar cells [7,8]. Organic-inorganic hybrid perovskites are now one of the hottest topics in modern material science because of their many excellent properties, applied to various optoelectronic technologies, including high electron mobility, a considerable length of carriers' diffusion, a significant absorption coefficient, a high photoluminescence quantum yield, and low surface recombination velocity [9]. Among the various emerging applications, it has found radical success in photovoltaic power generation, particularly in the remarkable record of energy conversion efficiency, now becoming comparable to silicon and other state-of-the-art thin film technologies [10]. Organic-inorganic solar cells based on nano-scale materials have recently gained interest as a replacement for fossil fuels in achieving clean energy from the sun due to their lightweight, flexible, and inexpensive manufacturing processes [5]. It is well known that the mobility of charge carriers inside semiconducting materials is a very important parameter ruling the PCE of solar cells. High mobility of the charges in these materials will ensure efficient transfer of charge and collection at the electrodes, therefore reducing recombination of the charge carriers. Thus, perovskites, with their high electron mobility property, are considered excellent candidates for use in solar cell technologies. For example, due to its wide-spectrum perovskite material, methylammonium lead iodide ($MAPbI_3$) has been commonly used to fabricate high-efficiency solar cells. This material has lead (Pb) as the central cation,

iodine (I) as the anion, and methylammonium as the organic component [11]. This specific combination of organic-inorganic hybrid perovskite material forms a semiconductor material with excellent light-absorbing properties. These strategies suppress the recombination of photogenerated charge carriers in diverse ways and are beneficial in enhancing the performance of studies associated with photovoltaics [12]. On the other hand, the interface problem in the PSCs is one of the primary key factors in determining efficiency and stability. Because of this, their power conversion efficiency (PCE) remains a challenge to their use compared to traditional silicon-based solar cells [5,13]. Recent studies by Ali et al. [14] and Djeradi et al. [15] highlighted optimizing these materials through advanced interface engineering and machine learning-driven band gap predictions, achieving efficiencies exceeding 25% and providing critical insights into material stability and performance under varying conditions. These developments underscore the importance of tailored material combinations to push PSCs toward commercial viability.

The perovskite solar cell is composed of five components: a cathode based on a hole-transporting metal, a hole-transport layer (HTL), an absorption layer, an electron transport layer (ETL), and a transparent conductive oxide (TCO). Transport layers govern the working performance and efficiency of PSCs. The main function of the HTL is to collect the photo-generated holes from the absorption layer, transport them to the cathode, and block electrons. Therefore, the highest occupied molecular orbital (HOMO) of the hole transport layer (HTL) material should be slightly higher than the orbital of the perovskite absorber layer, like the graphene-based materials NiO, CuO, CuI, and Cu_2O. On the other hand, the primary function of an electron transport layer (ETL) is to collect the photogenerated electrons from the absorber layer and transport those toward the anode, in addition to blocking the holes. The HOMO and LUMO levels of the ETM material should be higher in energy than those of the perovskite absorption layer [16,17]. At present, PSCs are under high research interest because of their high efficiency, broad absorption spectra, intense optoelectronic performance, and fabrication flexibility with low-cost materials. The PCE of perovskite-based solar cells has already exceeded 25%, drawing initial interest [7,18].

However, there are several challenges to the sustainable commercialization of PSCs, such as their long-term stability and the considerable effort required to improve the PCE and scale up [15]. One of the most critical factors limiting PCE in organic/inorganic solar cells is the open-circuit voltage (V_{OC}) (3R1). A high V_{OC} signifies a larger potential difference across the cell, resulting in greater power output [19,20]. As a result, research efforts are focused on building new strategies to improve and enhance V_{OC} to achieve higher overall efficiency. Many strategies have been suggested to address these issues, such as using interlayers with organic electron or hole transfer materials, the incorporation of metal oxides with selective charge transport toward the charge-selective contact, and various combinations of inorganic materials [18,21]. Several hole and electron transport layers (HTL, ETL) materials with a perovskite absorber layer were employed to improve the performance of PSCs and their stability and cost-effectiveness [22,23]. For example, Yuhan Wu produced high-efficiency solar cells utilizing bromide (KBr) in poly (3,4-ethylene dioxythiophene):polystyrene sulfonate (PEDOT:PSS) as HTL to improve the cell's conductivity and interfacial charge transfer. Mikroyannidis and co-workers fabricated a $CH_3NH_3PbI_3$ perovskite solar cell using 1D PCBM nanorods as ETL to improve cell performance from 9.5% to 15.3% [23]. However, there are a lot of disadvantages to using organic materials such as ETL and HTL in PCS, such as lowered efficiency and reduced stability compared to inorganic alternatives, because of limited absorption range and poor charge carrier mobility [24]. Therefore, metal oxide materials such as ZnO, TiO_2, CeO_2, and GO have

been used to fabricate PCEs [18,25,26]. These materials are well-known as electron acceptors and transparent layers for applications in solar cells. For example, Bhattarai et al. [22] reported that the efficiency of poly(3-hexylthiophene) (P3HT)/titanium dioxide (TiO_2) nanorods hybrid bulk heterojunction (BHJ) and nanostructured zinc oxide (ZnO)/P_3HT hybrid solar cell is mainly dependent on the nanomorphology of the polymer/nanocrystal hybrid.

Amongst PSCs, hybrid- and lead (Pb)-based cells are the most investigated due to their exceptional optical and electrical properties, which lead to generating high efficiencies [20]. Over the years, PSCs' strength conversion efficiency has increased from 3.8% in 2009 to over 26% [9]. It is well-known that the correct choice and order of components in the device architecture of PSCs can help further enhance the efficiency of the devices [18,27]. Yella et al. [28] found that the nanocrystalline interface between TiO_2 and the perovskite layer demonstrated better efficiency for the extraction of electrons, which exhibited a PCE of 13.7%.

Stable and efficient PSCs have also been realized through the use of polymers. Polymers assume significant roles in PSCs as interfacial layers, encapsulation layers, and additives in the Perovskite's charge transport and active layers. Various polymers are employed and have been studied in terms of their design, synthesis, and integration into PSCs. Polymers help in enhancing morphology, thermal stability, suppression of recombination, moisture barrier ability, stability, and flexibility [29,30].

This article investigates the theoretical possibility of incorporating a methylammonium lead iodide ($MAPbI_3$) interlayer in the middle of the two layers of HTL and ETL (interfacial layers) to improve the performance of titanium dioxide (TiO_2)/graphene oxide (GO) perovskite solar cells. As one of the most promising materials, graphene-based materials have been critically reviewed for different sections like HTMs, ETMs, and materials for inorganic perovskite modification [31]. Based on various outstanding properties of graphene and graphene materials, their implementation in PSCs is also highly promising. In the preceding decade, 2D materials, especially graphene oxide (GO) with hybridization of promising structures, have drawn considerable attention for novel energy devices such as solar cells, owing to extraordinary electrochemical, mechanical, and stability attributes besides predictable charge transport [32,33]. For instance, Yadav et al. [34] showed how reduced graphene oxide (rGO) performs better as an HTL material in comparison to GO, paired with the lead-free double perovskite Cs_2SnI_6, to yield a PCE of 19.07% compared to 16.9% using GO. GO has a highly tunable bandgap that is highly variable with its structural arrangement and oxidation level; values range from as much as 4.77 eV in its oxidized form to a minimum of 1.1 eV following controlled reduction, presenting a wide range of electronic attributes for use in various optoelectronic purposes [35,36].

Furthermore, titanium dioxide, as a cheap, non-toxic, transparent, and readily available semiconductor, is commonly utilized as a photocatalyst [37–40] and electron-transport layer (ETL) in PSCs because of its ideal valence band position for efficient hole extraction and far higher conduction band electrons compared to those of other metal oxides, leading to efficient electron transfer to the ETL [26,41,42]. It also acts as a physical barrier to prevent direct contact between the perovskite absorber layer and the conducting substrate layer, thereby minimizing charge recombination. Bulowski et al. [26] emphasized the importance of optimizing the TiO_2 layer in inorganic $CsPbBr_3$ PSCs. The study indicates that TiO_2's stability and high optical transparency make it a popular choice for ETLs, primarily in inorganic devices.

The use of $MAPbI_3$ can be considered an essential component in the photovoltaic device's architecture, which impacts the charge transfer and collection by/with adjacent components and thus can greatly enhance cell efficiency [13]. When utilizing $MAPbI_3$ as the perovskite material, devices

that incorporate TiO_2 or SnO_2 as ETMs, combined with Spiro-OMETAD as the HTM, demonstrate impressive efficiencies exceeding 22%. However, the performance varies with different ETMs; for instance, using ZnO or PCBM in conjunction with Spiro-OMETAD results in lower efficiencies [14]. Furthermore, substituting Spiro-OMETAD with alternative HTMs such as PEDOT:PSS, Cu_2O, or CuSCN while maintaining TiO_2 as the ETM leads to notable changes in performance metrics. Specifically, the open-circuit voltage (V_{OC}) increases with the use of Cu_2O and CuSCN. At the same time, the short-circuit current density (J_{SC}) and fill factor exhibit variability, ultimately affecting the overall efficiency of the solar cells. These findings underscore the critical role that the selection of ETMs and HTMs plays in optimizing the performance of perovskite solar cells [14].

We utilize SCAPS-1D simulation, a well-established tool for simulating solar cell behavior, to explore the impact of the $MAPbI_3$ layer on various cell parameters. Our focus lies on understanding how this modification influences V_{OC}, PCE, and other key characteristics, aiming to elucidate the underlying mechanisms responsible for the observed efficiency improvements.

2. The simulated device construction and input parameter details

This section provides detailed information about the construction device and the input simulated parameters that were used to evaluate the performance of the construction cell. The SCAPS-1D software program was used to study the factors that may limit the solar cell's performance. This simulated software is a one-dimensional solar cell simulation program developed by the Department of Electronics and Information Systems (ELIS) at the University of Gent, Belgium [15].

This software has been regularly used as a simulator in solar cells research since 2002. It demonstrates accuracy in predicting solar cell performance by comparing experimental results with theoretical predictions [43]. That makes it a reliable tool for the simulation and optimization of solar cell structures. In fact, it can be used as a valuable tool in the first stages of research building and investigation since it is particularly economical and can deal with complex multi-layer structures. Conversely, the SCAPS-1D model might be time-consuming and typically necessitates material parameters with complete accuracy, which can be hard to achieve for new or less-researched materials. In addition, it has limits in simulating some material features, particularly those related to three-dimensional effects like light trapping and spatial inhomogeneities. The model also requires an ample background in semiconductor physics, which can be an obstacle for new individuals or interdisciplinary scientists [44].

The program is based on solving Poisson's and continuity equations for the free electrons and holes in the conduction and valence bands, respectively. Figure 1 shows the schematic diagram of the designed and suggested solar cell, which consists of the front contact electrode (SnO_2:F)/ETL (TiO_2)/absorber layer ($MAPbI_3$)/HTL (GO)/back contact electrode (*Au*).

The suggested device configurations are designed by employing diverse materials with distinct layer thicknesses. Tables 1, 2, and 3 show the input parameters used in SCAPS simulations for each layer, which are selected carefully based on the valuable findings in previous literature to evaluate solar cell performance [45–47]. In the proposed solar cells, TiO_2 and GO serve as electron and hole transport layers, respectively, while $MAPbI_3$ acts as the absorbing material between the ETL and the HTL.

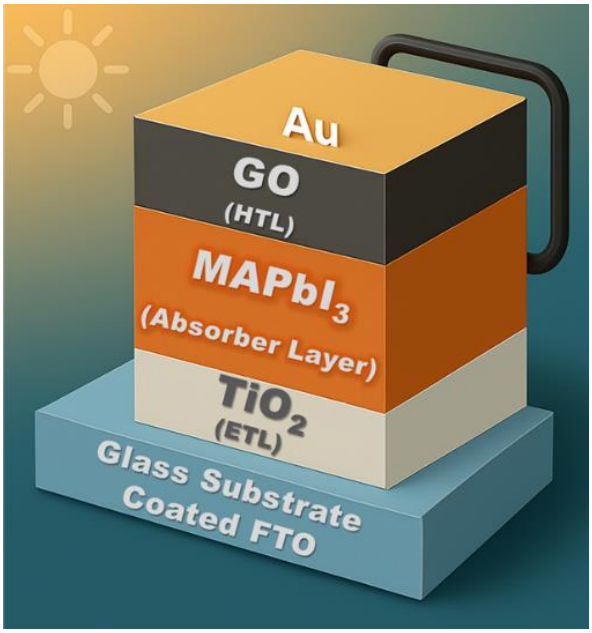

Figure 1. Schematic of the GO/$MAPbI_3$/nc-TiO_2 solar cells.

Table 1. Simulation parameters of each layer of the proposed solar cell.

Material characteristics	TiO_2	$MAPbI_3$	GO
Thickness of each material (μm)	0.10	0.40	0.20
Bandgap of the material (eV)	3.25	1.55	3.25
Material electron affinity (eV)	4.20	3.95	1.90
Dielectric permittivity of the material (relative)	10.00	6.50	3.00
Conduction band effective density of states ($1/cm^3$)	2.00×10^{18}	3.97×10^{18}	2.20×10^{21}
Valence band effective density of states ($1/cm^3$)	1.80×10^{18}	3.97×10^{18}	1.80×10^{21}
Electron mobility (cm^3/Vs)	20.00	2.00	1.00×10^{2}
Hole mobility (cm^3/Vs)	10.00	2.00	3.00×10^{2}
Shallow uniform donor density ND ($1/cm^3$)	1.00×10^{16}	10.00×10^{13}	0.00
Shallow uniform acceptor density NA ($1/cm^3$)	0.00	0.00	1.00×10^{16}
Defect density Nt (cm^{-3})	1.00×10^{15}	10.00×10^{14}	10.00×10^{14}

With the help of SCAPS-1D software, we aim to understand the influence of various factors that affect the performance of the designed solar cell device, including the presence of $MAPbI_3$, the thickness of the $MAPbI_3$ layer, the work function of the back contact, and temperature. Optimizing these factors leads to significant improvement in the overall outputs of the PSC, which can be assisted by the outcome PV parameters such as high open-circuit voltage (V_{OC}), short-circuit current density (J_{SC}), FF, and PCE.

Table 2. Simulation parameters of the back and front contacts of the proposed device.

Parameter	Back contact (Au electrode)	Front contact (SnO_2:F electrode)
Surface recombination velocity of electrons (cm/s)	1.00×10^5	1.00×10^5
Metal-work function (eV)	5.10	4.40

Table 3. Interface defect input parameters.

Interface	Go/$MAPbI_3$	$MAPbI_3/TiO_2$
Defect type	Neutral	Neutral
Energetic distribution	Single	Single
Capture cross-section for electrons (cm^{-2})	10^{-19}	10^{-19}
Capture cross-section for holes (cm^{-2})	1×10^{-19}	10^{-19}
Reference for defect energy level	Above the VB maximum	Above the VB maximum
Energy concerning reference (eV)	0.6	0.6
Total density (cm^{-3})	1×10^{10}	1×10^{10}

3. Results

3.1. Pre-optimization performance of TiO_2/$MAPbI_3$/GO solar cells

It is well known that the performance of solar cells is dependent on a wide variety of factors, all of which come together to the effective and efficient functioning of a device [48]. It is imperative that an attempt is made to understand these factors in depth to achieve the best fit for the design of a solar cell. One critical step in this process is the review of solar cells under some controlled initial conditions so that a reference point can be used for their further performance assessment and optimization. Hence, in this study, we established some initial conditions for reviewing the baseline performance of the device to ensure comparison consistency under different scenarios. We initially used a back-contact Au electrode with an adjusted operating temperature of the solar cells at 300 K and $MAPbI_3$ bandgap and thicknesses of 1.6 eV and 0.2 μm, respectively.

Figure 2 shows the current density-voltage (*J*—*V*) curve simulated for TiO_2/$MAPbI_3$/GO solar cells under such initial conditions of illumination. The *J*—*V* curve is of high importance since it gives us knowledge about the electrical performance of the device and points toward certain possible ways for improving it in future optimization.

The short-circuit current (I_{SC}), open-circuit voltage (V_{OC}), and maximum output power (P_{max}) are critical parameters for evaluating the performance of solar cells. PCE is determined by the ratio of the maximum output power to the power of the incident light (Pin) (see Eq 1). Similarly, the fill factor (FF) is an important indicator of the quality of the solar cell's electrical characteristics (see Eq 2). Based on the findings presented in Figure 2, the TiO_2/$MAPbI_3$/GO solar cell exhibited a V_{OC} of 1 V, *J*sc of 14.7 mA/cm², and a maximum output power (P_{max}) of 11.63 watts. Utilizing Eqs 1 and 2, the calculated maximum PCE% was 11.6%, with a fill factor of 78.5%. These results were achieved under the initial conditions and will serve as a reference point for designing solar cells with enhanced efficiency.

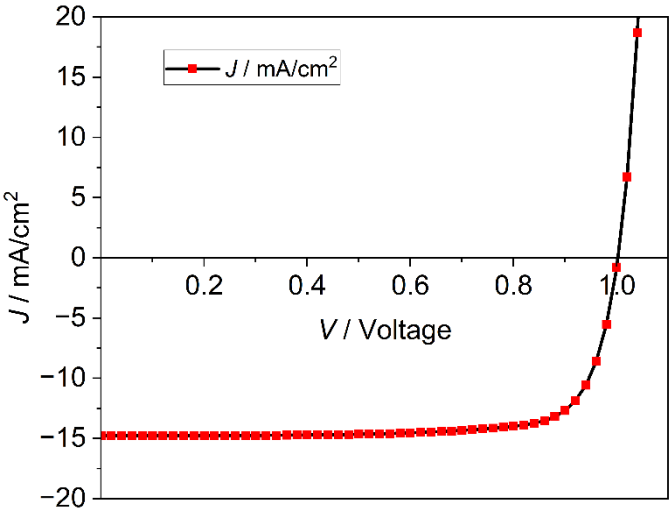

Figure 2. Current density-voltage (*J–V*) plot for the SnO_2:F/TiO_2/$MAPbI_3$/GO/Au under initial structure conditions.

$$PCE = \frac{I_{sc} V_{oc} FF}{P_{light}} \quad (1)$$

$$FF = \frac{P_{max}}{I_{sc} V_{oc}} = \frac{I_m V_m}{I_{sc} V_{oc}} \quad (2)$$

Table 4 summarizes the key parameters of the solar cells, presenting the pre-optimized results for the TiO_2/$MAPbI_3$/GO solar cells. These baseline values provide a foundation for further optimization and performance enhancement efforts.

Table 4. Main parameters of TiO_2/$MAPbI_3$/GO solar cells.

Parameter	J_{SC} (mA/cm^2)	V_{OC} (V)	FF (%)	PCE (%)
Pre-optimized results	14.7	1	78.5	11.6

Figure 3 presents the preliminary simulation results of the external quantum efficiency (EQE) for the TiO_2/$MAPbI_3$/GO-based photovoltaic cells. The EQE is the percentage of photogenerated electron-hole pairs in the absorber layer of the PV device with respect to the incident photons that produced them, collected as electrical current.

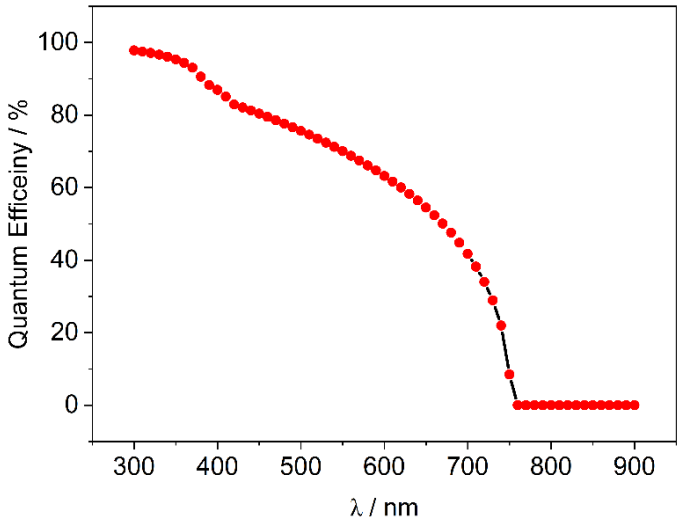

Figure 3. Quantum efficiency for the SnO_2:F/TiO_2/$MAPbI_3$/GO/Au under initial structure conditions.

Mathematically, the EQE can be written as the ratio of the number of collected charge carriers to the number of incident photons, where E_{photon} describes the energy of incident photons at a given wavelength λ, and P(λ) is the incident light power at that particular wavelength, as shown in Eq 3.

$$\mathrm{EQE} = \frac{E_{\mathrm{photon}}}{q} \times \frac{I_{\mathrm{sc}}}{P(\lambda)} \tag{3}$$

Indeed, in Figure 3, we observe a slight drop in EQE at the wavelength range of 300–350 nm. As it increases in wavelengths from 350 to 750 nm, EQE gently reduces from 85% to 5%. Beyond 750 nm, EQE remains unscathed and stays almost constant at around 5% up to 900 nm. Therefore, this wavelength dependence of EQE shows the light absorption properties of the $MAPbI_3$ layer. The main drop in EQE for lower wavelengths of approximately 300–350 nm has to be ascribed to a reduced absorption or carrier collection in that window. The larger drop from 350 to 750 nm is due to the intrinsic reduction of the $MAPbI_3$ light absorption efficiency with increasing wavelength, common to materials of well-defined absorption. The flatness of the EQE at long wavelengths means that absorbed photons >750 nm hardly contribute to electron-hole pair generation, presumably because $MAPbI_3$ has a much lower absorption coefficient in this region. In fact, these results are important because they present an insight into how the material properties of $MAPbI_3$ affect the overall solar cell performance and guide further optimization efforts that are directed centrally toward improving the efficiency across the entire spectrum.

3.2. Effect of $MAPbI_3$ thickness on performance of TiO_2/$MAPbI_3$/GO solar cells

The thickness of layers in solar cells is of high relevance to the mechanisms of separation and recombination of photogenerated charge carriers: for efficient charge carrier separation and collection, the diffusion lengths of electrons and holes in materials should be larger than the thickness of the components of a solar cell [49,50].

Figure 4 illustrates the effect of the $MAPbI_3$ layer thickness on the performance of TiO_2/$MAPbI_3$/GO solar cells.

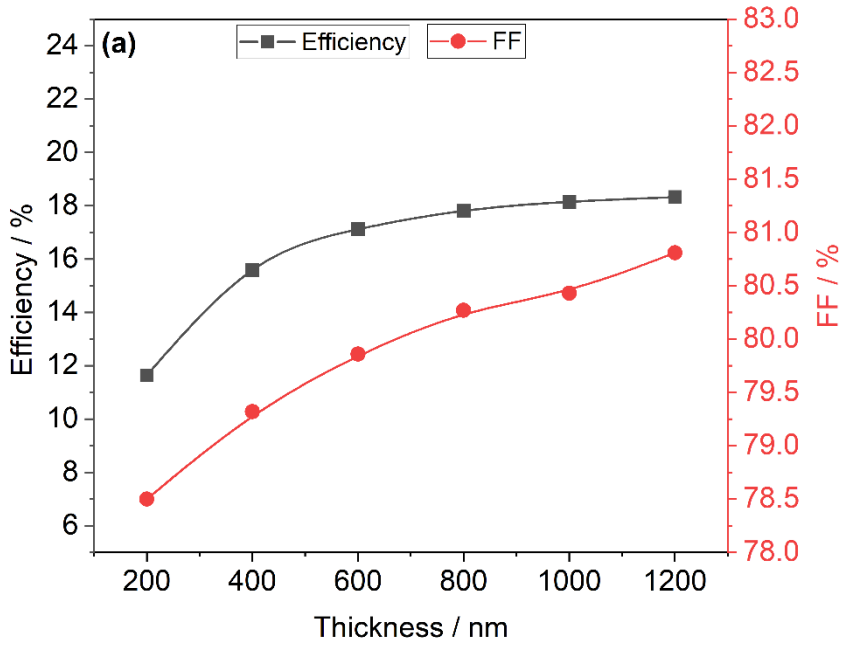

(a)

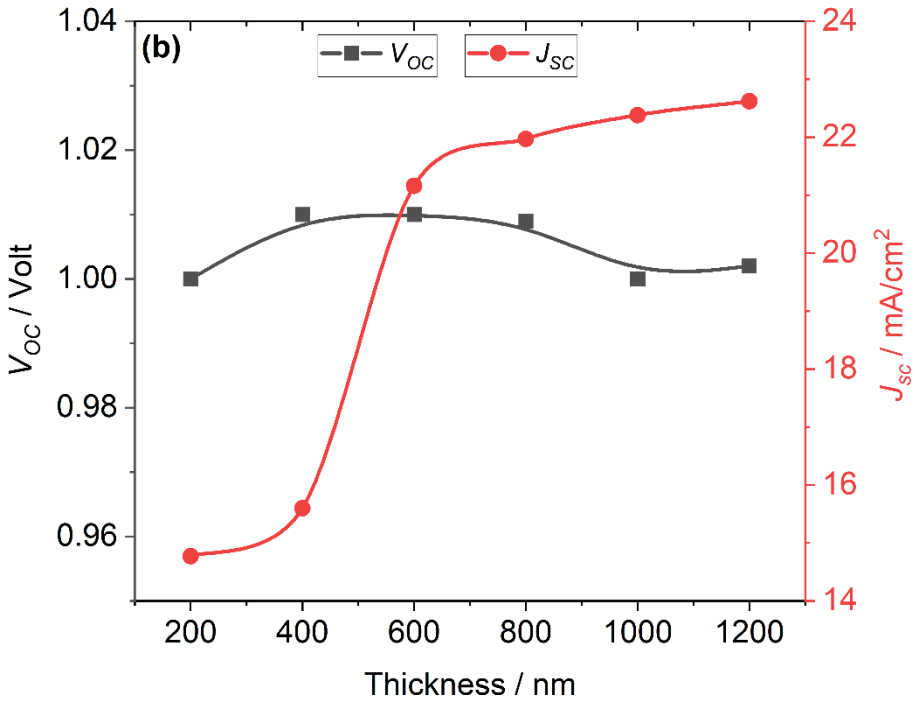

(b)

Figure 4. Effect of variation of increasing absorber layer thickness on efficiency and FF (a) and *J*sc and *V*oc (b) of TiO_2/$MAPbI_3$/GO solar cells.

As shown in Figure 4, increasing the $MAPbI_3$ thickness leads to a gradual improvement in the J_{SC}, PCE, and FF of the solar cells up to a thickness of 700 nm. This improvement indicates enhanced

electron-hole pair generation within the $MAPbI_3$ layer. However, when the $MAPbI_3$ thickness exceeds 700 nm, the increases in these performance metrics slow down or become saturated. This saturation occurs because, at greater thickness, the rate of electron-hole recombination begins to surpass the generation rate within the thicker absorption layer. Figure 4b illustrates the initial increase in the V_{OC}, which suggests a reduction in charge carrier recombination. However, as the thickness of the absorber layer increases further, a decrease in V_{OC} is observed. This behavior can be attributed to the dependence of V_{OC} on both the J_{SC} and the dark saturation current (J_o). The relationship between V_{OC}, J_{SC}, and Jo is described by the Shockley-Queisser equation (Eq 4) [51].

$$V_{oc} = \frac{nK_BT}{q}\left[ln(1 + \frac{J_{sc}}{J_o} - \frac{V_{oc}}{J_sR_{sh}}\right] \quad (4)$$

where V_{OC} is the open circuit voltage, n is the ideality factor, q is the elementary charge, K_B is the Boltzmann constant, Jo is the reverse current, R_{sh} is the shunt resistance, T is the temperature (absolute), and q is the electric charge. As the thickness of the $MAPbI_3$ absorber layer increases, the dark saturation current (J_o) also increases. This leads to a higher probability of charge carrier recombination, ultimately resulting in a decrease in V_{OC} [52].

3.3. Effect of $MAPbI_3$ band gap on the performance of perovskite solar cells

The bandgap of the perovskite layer is essential for the overall performance of perovskite solar cells (PSCs). Numerous studies have demonstrated that the efficiency of these cells is greatly influenced by the band gap, which governs critical processes such as light absorption and charge carrier generation. A smaller band gap might allow for broader light absorption. However, it often results in limited absorption of incoming light. This, coupled with an increased likelihood of charge carrier recombination, significantly reduces the efficiency of solar cells [53].

In our case, the effect of varying the band gap of the $MAPbI_3$ layer from 1.48 to 1.6 eV is studied using SCAPS-1D simulation software, as shown in Figure 5. The results reveal a complex relationship between the band gap and other solar cell parameters. At a band gap of 1.48 eV, the maximum short-circuit current density (J_{SC}) reaches 18.7 mA/cm². However, as the band gap increases, J_{SC} gradually decreases (Figure 5a). This decline can be attributed to the reduced generation of electron-hole pairs as the band gap widens, limiting the photocurrent.

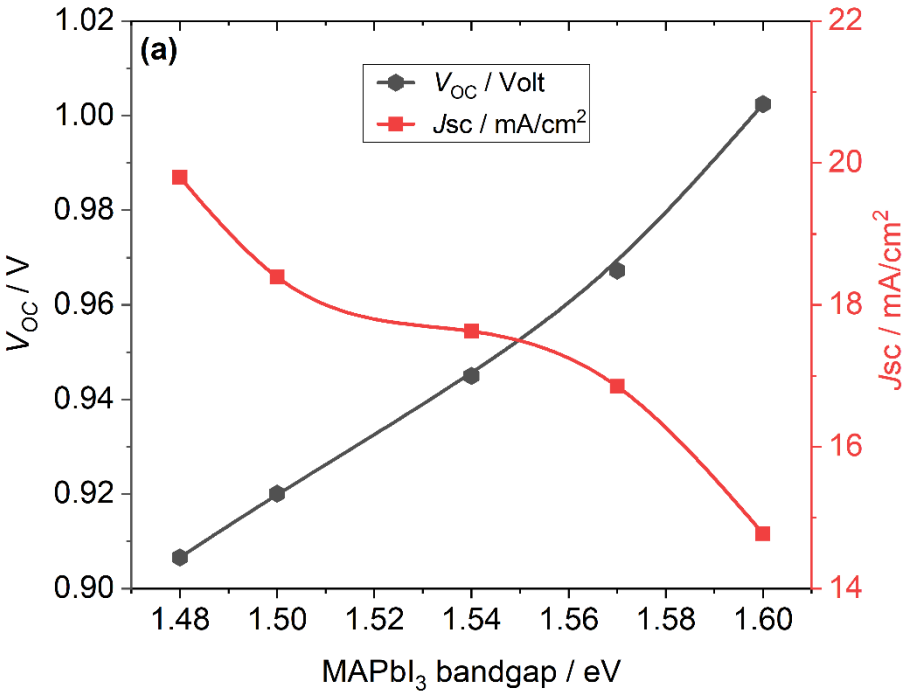

(a)

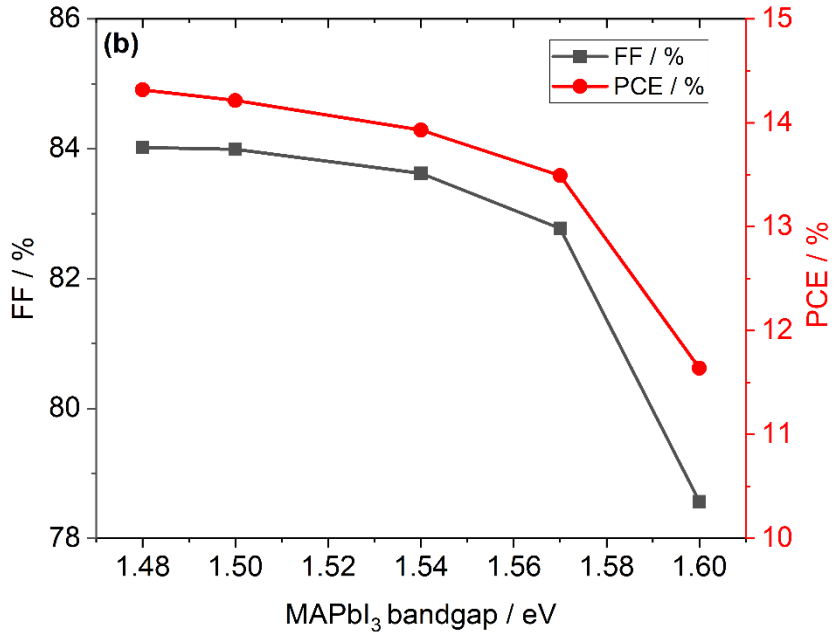

(b)

Figure 5. Effect of variation of increasing $MAPbI_3$ bandgap on (a) *J*sc and V_{OC} and (b) efficiency and FF of $TiO_2/MAPbI_3/GO$ solar cells.

Conversely, the V_{OC} shows the opposite trend. It peaks at 1 V with a 1.6 eV band gap and decreases to 0.9 V at a 1.1 eV band gap. A larger band gap suppresses electron-hole recombination, leading to an increase in V_{OC}. However, this increase in V_{OC} comes at the cost of a reduced *J*sc, as fewer charge carriers are generated at higher band gaps.

The balance between the two parameters J_{SC} and V_{OC} strongly dictates the overall efficiency and fill factor of the solar cells. While an increase in V_{OC} usually improves the fill factor, the simultaneous decrease in *J*sc can negate these gains, leading to a net reduction in performance. The fill factor, which reflects the quality of the solar cell, initially benefits from reduced recombination at higher band gaps, but this improvement is offset by the declining J_{SC}, which can ultimately diminish overall efficiency.

As shown in Figure 5b, the maximum values of both efficiency and fill factor are produced at the band gap of 1.5 eV, after which they begin to decline. The highest efficiency of 14.37% is observed at a band gap of 1.5 eV, suggesting an optimal balance between J_{SC} and V_{OC}. Notably, we observe a broad peak in fill factor within a band gap interval from 1.48 to 1.54 eV, suggesting this interval offers the optimal trade-off between charge carriers generated and recombination losses. Outside this interval, decreases in efficiency and fill factor show decreasing returns by further raising the band gap. Based on our data, although increasing the band gap of the $MAPbI_3$ layer can improve V_{OC} and suppress recombination loss, it also decreases J_{SC} and can have a negative influence on overall efficiency and fill factor. The band gap optimization plays a key role in realizing optimized performance in perovskite solar cells, with peak efficiency at 1.5 eV being a key reference point for future designs and optimization in PSCs.

3.4. Influence of defect and doping densities in $MAPbI_3$ on perovskite solar cell performance

Figure 6 shows the influence of changing defect density (10^{13} to 10^{19} cm^{-3}) and doping density (10^{17} to 10^{21} cm^{-3}) of the $MAPbI_3$ absorber layer PCE of a SnO_2:F/TiO_2/$MAPbI_3$/GO/Au perovskite solar cell. The data presented show that PCE remains relatively stable at around 11.7% at defective density levels up to 10^{15} cm^{-3}. Beyond this threshold (Figure 6a), efficiency declines markedly, falling from 11.74% at 1×10^{13} cm^{-3} to 0.40% at 1×10^{19} cm^{-3}. This steep decline is explained by the enhanced defect-mediated recombination, speeding up the loss of photogenerated charge carriers, thus decreasing the electrical output of the cell. Likewise, doping concentration (Figure 6b) also shows minimal influence on PCE up to a concentration of 10^{20} cm^{-3} with a value close to 11.5% [54]. Similarly, doping density (Figure 6b) has a limited impact on PCE up to 10^{20} cm^{-3}, maintaining values near 11.5%. However, at 1×10^{21} cm^{-3}, PCE decreases to 9.89% from 11.66% at 1×10^{17} cm^{-3}. Excessive doping likely disrupts the internal electric field within the $MAPbI_3$ layer, impeding charge carrier transport and diminishing efficiency [55]. These trends underscore optimizing defect and doping levels to balance charge recombination and transport properties for high-performance perovskite solar cells [56].

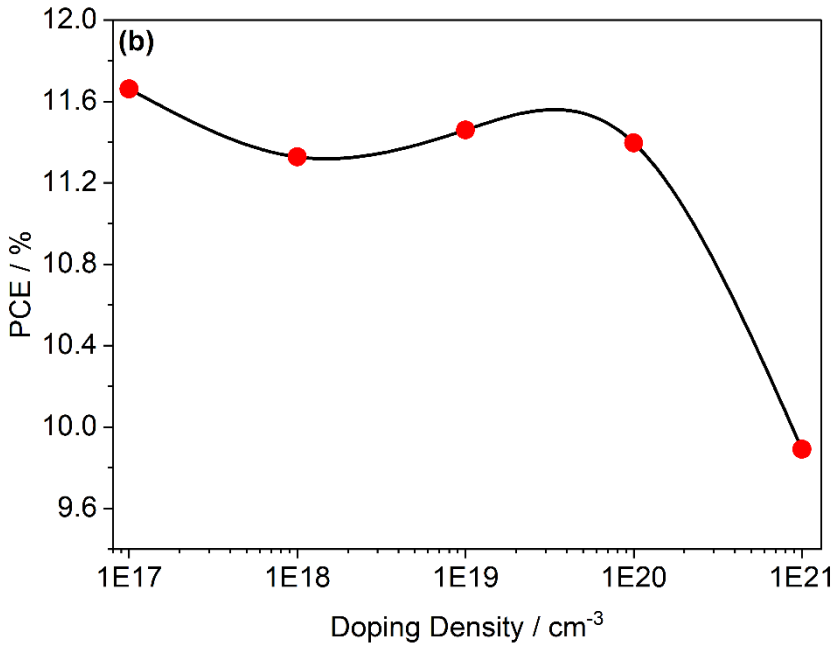

(a)

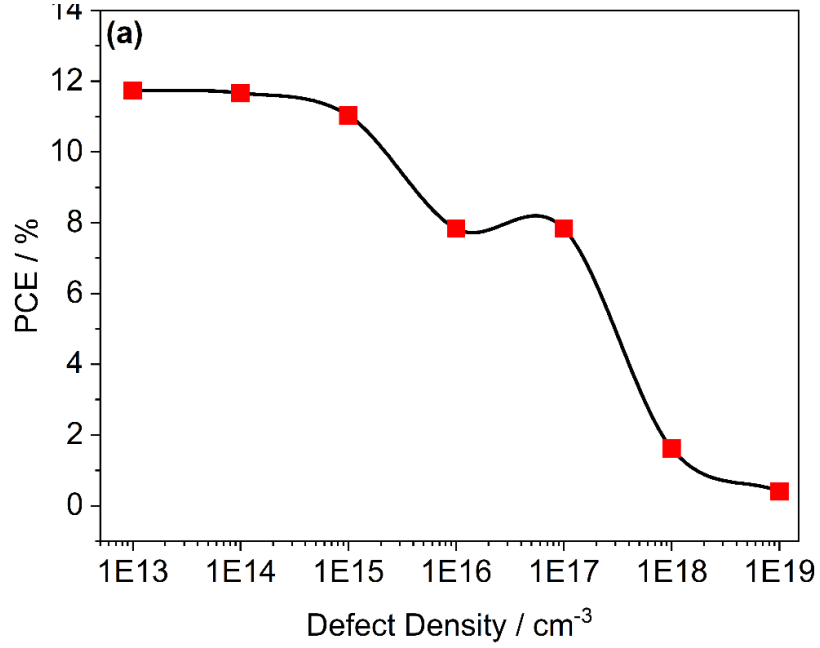

(b)

Figure 6. The effect of concentration of (a) defect density and (b) doping density in the $MAPbI_3$ layer.

3.5. Effect of temperature on the performance of devices

Improving the thermal stability of perovskite solar cells (PSCs) and mitigating the negative impact of temperature on their performance has required extensive efforts in developing new materials and device architectures. According to the literature, V_{OC} in PSCs is the most sensitive and readily varies with temperature change, thereby directly influencing the overall efficiency of the cells. Every

temperature dependence is majorly brought about by changes in the band gap, electron and hole mobilities, and concentrations of charge carriers in various parts of the solar cell [10,57]. Temperature-induced atomic vibrations in the semiconductor increase interatomic distances, which are quantified by the material's linear temperature coefficient.

Table 5 shows the effect of temperature on the performance of TiO_2/$MAPbI_3$/GO solar cells when the thickness of $MAPbI_3$ was 1.2 μm. As shown in Table 5, a significant reduction in V_{OC} is observed with increasing temperature, while the short-circuit current (J_{SC}) remains relatively stable, with a slight increase at higher temperatures. These trends can be explained by Eq 3, which highlights the inverse relationship between the reverse saturation current density (J_o) and the open-circuit voltage. With an increase in temperature, there are more generations of electron-hole pairs, leading to a rise in J_o along with a reduction in V_{OC}. Furthermore, recombining hole-electron pairs within solar cells plays a crucial role in decreasing V_{OC} as a function of high temperature. Larger interatomic spacing of the material, for example, in $MAPbI_3$, reduces the band gap and can be considered as one of the factors that provide ground for the observed decrease of PCE with the rise in temperature. This can be described by Varshni's Eq (5):

$$E_{g(T)} = E_{g(0)} - (\alpha T^2)/(\beta + T) \tag{5}$$

where β and α are the material constants, T is the temperature, and $E_{g(0)}$ is the bandgap at 0.0 K. Temperature elevation in TiO_2/$MAPbI_3$/GO solar cells increases vibrations between atoms, lattice dilation, and stronger electron–phonon coupling between their constituents. This lowers the bandgap and raises intrinsic carrier concentrations, leading to higher recombination rates and a corresponding reduction in V_{OC}. Concurrently, an increase in Jsc from 22.40 to 22.74 mA/cm² is observed. This is due to red shifting of the absorption edge resulting from bandgap narrowing, which facilitates the ability of the cell to capture lower-energy photons, and a small contribution from carriers formed due to thermal energy [58].

In contrast, the fill factor (FF) exhibits a more complex relationship with temperature. With an increase in temperature from 300 to 340 K, FF increases due to increased mobility of charge carriers, which, in turn, allows greater current to pass through the device; beyond 340 K, it falls due to increased recombination of the charge carriers before they reach the electrodes. This balance between mobility and recombination determines the unique performance of PSCs at different temperatures. These findings are in good agreement with previously reported works [10,57], which have illustrated the crucial role of temperature in dictating both electronic properties and efficiencies of perovskite materials. The decrease of V_{OC} and FF at elevated temperatures, along with the rather stable J_{SC}, would recommend considering thermal management methodologies to stabilize PSCs' efficiency under practical operating conditions.

Table 5. Parameters of TiO_2/$MAPbI_3$/GO solar cells as a function of temperature.

Temp. (K)	PCE%	FF%	J_{SC} (mA/cm^2)	V_{OC} (Volt)
300	18.10	81.10	22.40	1.10
320	17.70	81.60	22.50	0.96
340	17.10	81.80	22.60	0.90
360	16.20	81.60	22.70	0.87
380	15.22	81.01	22.73	0.82
400	14.10	79.90	22.74	0.77

3.6. Effect of back-contact work function

The characteristics of the interracial layers between the electron transport layer (ETL), hole transport layer (HTL), and metal contacts (both back and front contacts) influence the stability of perovskite solar cells and the recombination probability of electrons and holes. To overcome these problems, selecting appropriate materials with well-aligned energy levels is vital to minimizing the defects formed at these interfaces. Figure 7 shows the efficiency of our simulated solar cell using six different metal materials selected as the bottom electrodes for the simulation test of different back contacts. These metals are aluminum (4.2 eV), tungsten (4.3 eV), copper (4.6 eV), silver (4.7 eV), iron (4.8 eV), and gold (5.1 eV). We chose these metals because they're commonly used in PSC designs, and their work functions align well with the energy levels needed for effective charge extraction in our device setup, particularly with the GO (HTL) [17,59].

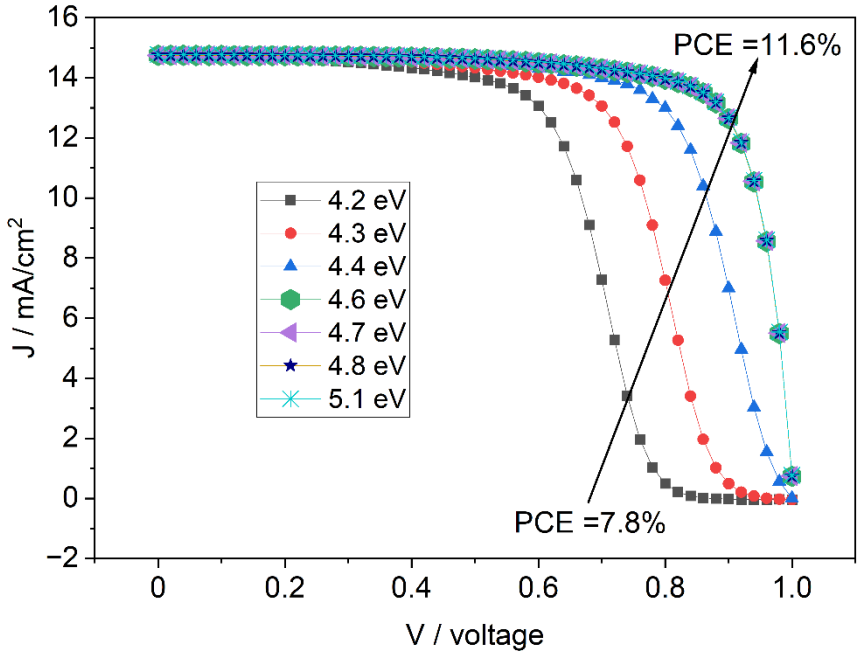

Figure 7. Effect of metal work function on device performance.

As shown in Figure 7, the PCE of TiO_2/$MAPbI_3$/GO solar cells climbs noticeably from 7.9% to 11.6% as the back-contact work function increases from 4.2 eV (aluminum) to around 4.6 eV (copper). Beyond 4.6 eV, the efficiency levels off, showing little change up to 5.1 eV (gold). This suggests that

a work function of about 4.6 eV or higher is ideal for minimizing energy barriers at the GO/electrode interface, which helps holes move more efficiently and reduces recombination losses [60]. The plateau in PCE at higher work functions indicates that once the metal's Fermi level aligns well with the HOMO of the GO layer, further increases do not add much to performance [57].

3.7. Effect of the thickness of TiO_2 and GO layers

In general, thicker or thinner layers in solar cells usually affect the performance of the charge transport efficiency, optical absorption, and the quality of interfaces created at different junctions between the HTL and ETL or with electrodes. Figure 8 shows the impact of changing the HTL and ETL thickness on the performance of the designed solar cells. The TiO_2 (ETL) and GO (HTL) thicknesses have been altered from 0.05 to 1 μm to explore the performance of PSCs. The data reveal that the PCE remains relatively stable across the tested thickness range, with only a slight reduction observed. This indicates that the electrical performance of the PSC is not thickness-dependent in the range of interest [45] for the ETL and HTL thickness when the $MAPbI_3$ absorber layer is optimized. The minimal variation in PCE implies that factors such as charge carrier mobility and interfacial recombination are not significantly compromised by thicker or thinner layers in this context. This behavior could be attributed to the optimal intrinsic properties of TiO_2 and GO, which maintain efficient charge extraction and transport even at varying thicknesses. This result is consistent with previous reports from other research groups, indicating that the absorber layer's properties primarily dictate PSC performance when transport layers are sufficiently thin, which ensures efficient charge extraction [16,52].

To ensure consistency and reproducibility in the device fabrication process, a thickness of 200 nm was selected as the standard for both the HTL and ETL during subsequent optimizations. This choice strikes a balance between practical manufacturability and performance stability, while also aligning with findings from prior studies that identify this range as optimal for minimizing resistive losses and maximizing interfacial contact quality [45].

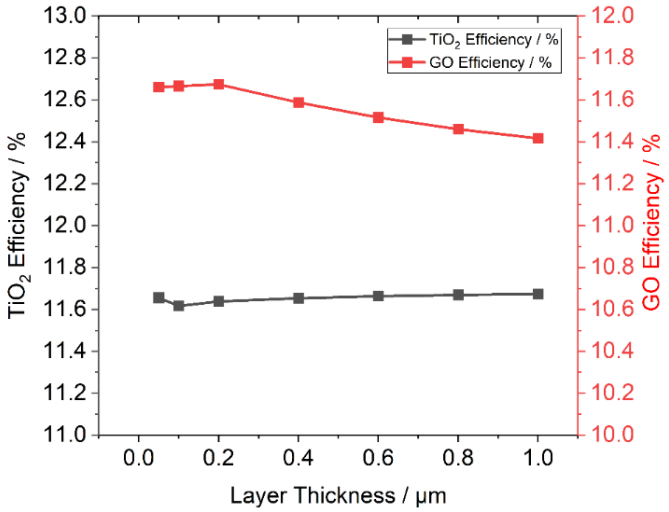

Figure 8. Effect of thickness of charge transport layers on the device performance.

3.8. Optimized TiO_2/$MAPbI_3$/GO solar cells

The optimization of the SnO_2:F/TiO_2/$MAPbI_3$/GO/Au structure was achieved through fine-tuning the $MAPbI_3$ (methylammonium lead iodide) layer, leading to a significant improvement in the solar cell's performance. The initial structure of the $MAPbI_3$ layer featured a thickness of 0.2 μm and an energy gap of 1.6 eV. However, in the optimized design, the thickness was increased to 1.2 μm, while the band gap was slightly reduced to 1.5 eV. These adjustments had a profound impact on the overall efficiency and quantum efficiency of the device, as shown in the *J*—*V* and quantum efficiency characterizations in Figure 9a and b, respectively.

The PCE of the optimized device increased by over 10%, reaching 20.8% compared to the initial structure's 13.79%. Moreover, the optimized device demonstrated a roughly 30% increase in quantum efficiency (Figure 9a), which remained stable across different conditions when compared to non-optimized solar cells. This consistency in quantum efficiency highlights the robustness of the optimization strategy.

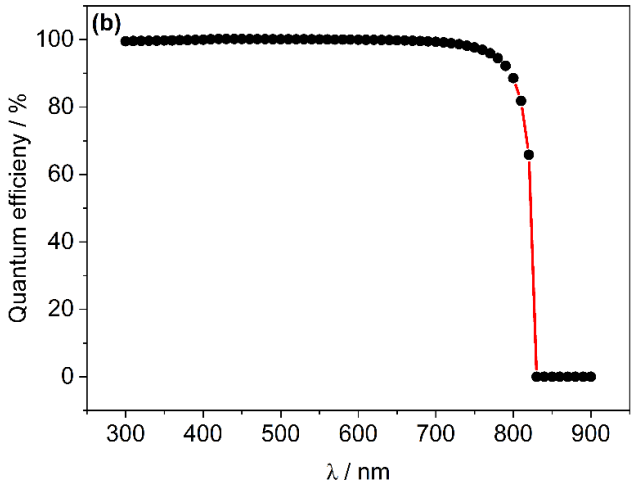

(a)

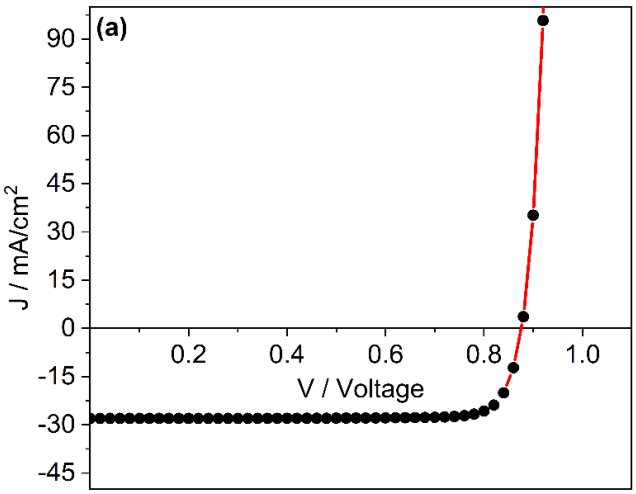

(b)

Figure 9. Optimized (a) current voltage (*J*—*V*) characteristics and (b) quantum efficiency curve of SnO_2:F/TiO_2/ $MAPbI_3$/GO solar cells.

The principal driving factor behind this efficiency boost is the independently increased thickness and narrowed bandgap of the $MAPbI_3$ layer. The optimized SnO_2:F/TiO_2/$MAPbI_3$/GO/Au solar cell reached a peak PCE value of 21% at a thickness of 1.2 μm and a band gap of 1.5 eV. This can be explained by enhanced sunlight absorption, since a thicker $MAPbI_3$ layer can catch more photons, resulting in increased electron-hole pair generation. The optimized thickness and band gap also optimize charge separation at interfaces between materials, minimizing losses due to recombination and charge transport.

The improved electron-hole pair generation and efficient charge separation at interfaces are thought to be responsible for contributing to the enhanced increases in PCE. The band gap in $MAPbI_3$ decreases from 1.6 to 1.5 eV, enabling more efficient absorption of lower energy photons, while the increased thickness ensures more sunlight is absorbed by the active layer. The combined effects serve to optimize solar cells' current generation and overall efficiency. It should be noted that our EQE data reported here appear comparable to those reported in prior published theoretical and experimental studies, further validating the veracity of our simulation data [61,62]. This structural optimization, especially within the $MAPbI_3$ layer, thus signifies a landmark progress in enhancing perovskite solar cell efficiency and stability.

4. Conclusions

This study demonstrates the significant potential of TiO_2/$MAPbI_3$/GO PSCs through systematic optimization using SCAPS-1D simulations. By fine-tuning the $MAPbI_3$ interlayer thickness (1.2 μm) and bandgap (1.5 eV), the device achieved a remarkable PCE of 20.8% and an FF of 80.5%, representing a substantial improvement over the initial configuration (11.6% PCE). These enhancements stem from optimized charge carrier generation and reduced recombination at the interfaces, underscoring the critical role of absorbing layer engineering in PSC performance. Beyond efficiency, this work highlights the economic and environmental advantages of the proposed design. The use of low-cost, abundant materials (TiO_2 and GO) and minimized $MAPbI_3$ consumption aligns with scalable manufacturing, while the reduced reliance on rare or toxic components supports sustainable photovoltaic development. However, addressing long-term stability remains essential for commercial viability, suggesting future research into encapsulation techniques or lead-free alternatives such as $CsSnI_3$ or double perovskites to reduce toxicity and environmental concerns. Collectively, these findings position TiO_2/$MAPbI_3$/GO PSCs as a promising pathway toward high-performance, cost-effective, and environmentally conscious solar energy solutions, bridging the gap between laboratory innovation and real-world application.

Use of AI tools declaration

In preparing this document, the authors did not utilize any AI tool.

Acknowledgments

Hmoud Al Dmour would like to acknowledge the support of the Deanship of Scientific Research of Mutah University through research project #339/2020. The authors are also thankful to Prof. Marc Burgelman, University of Gent, Belgium, for providing the SCAPS-1D software for our study.

Conflict of interest

The authors declare that they have no conflicts of interest.

Author contributions

Hmoud Al Dmour and Osama Y. Al-Madanat contributed to the conceptualization of the study. Hmoud Al Dmour, Rakan M. Altarawneh, Emad K. Jaradat, and Beddiaf Zaidi conducted formal analysis and simulations. Hmoud Al Dmour, Osama Y. Al-Madanat, Emad K. Jaradat, and Beddiaf Zaidi were responsible for processing both experimental and theoretical data. Hmoud Al Dmour and Osama Y. Al-Madanat analyzed the results. Rakan M. Altarawneh, Emad K. Jaradat, and Beddiaf Zaidi designed the figures. Bonginkosi V. Kheswa validated the results and gave technical advice on material characterization. Hmoud Al Dmour and Osama Y. Al-Madanat prepared the initial draft of the manuscript. Osama Y. Al-Madanat and Rakan M. Altarawneh revised the final version. Hmoud Al Dmour and Osama Y. Al-Madanat provided supervision throughout the project.

References

1. Olabi AG, Abdelkareem MA (2022) Renewable energy and climate change. *Renew Sustain Energy Rev* 158: 112111. https://dx.doi.org/10.1016/j.rser.2022.112111
2. Jiries A, Al-Nasir F, Hijazin TJ, et al. (2022) Polycyclic aromatic hydrocarbons in citrus fruit irrigated with fresh water under arid conditions: Concentrations, sources, and risk assessment. *Arab J Chem*, 15. https://dx.doi.org/10.1016/j.arabjc.2022.104027
3. Al-Dmour H, Alzard RH, Alblooshi H, et al. (2019) Enhanced energy conversion of Z907-based solar cells by cucurbit[7]uril macrocycles. *Front Chem*, 7. https://dx.doi.org/10.3389/fchem.2019.00561
4. Kannan N, Vakeesan D (2016) Solar energy for future world: A review. *Renew Sustain Energy Rev* 62: 1092–1105. https://dx.doi.org/10.1016/j.rser.2016.05.022
5. Solak EK, Irmak E (2023) Advances in organic photovoltaic cells: A comprehensive review of materials, technologies, and performance. *RSC Adv* 13: 12244–12269. https://dx.doi.org/10.1039/D3RA01454A
6. Osman AI, Chen L, Yang M, et al. (2023) Cost, environmental impact, and resilience of renewable energy under a changing climate: a review. *Environ Chem Lett* 21: 741–764. https://dx.doi.org/10.1007/s10311-022-01532-8
7. Li G, Li M, Taylor R, et al. (2022) Solar energy utilisation: Current status and roll-out potential. *Appl Therm Eng* 209: 118285. https://dx.doi.org/10.1016/j.applthermaleng.2022.118285
8. Kamarulzaman A, Hasanuzzaman M, Rahim NA (2021) Global advancement of solar drying technologies and its future prospects: A review. *Sol Energy* 221: 559–582. https://dx.doi.org/10.1016/j.solener.2021.04.056
9. Roy P, Kumar Sinha N, Tiwari S, et al. (2020) A review on perovskite solar cells: Evolution of architecture, fabrication techniques, commercialization issues and status. *Sol Energy* 198: 665–688. https://dx.doi.org/10.1016/j.solener.2020.01.080
10. Correa-Baena J-P, Abate A, Saliba M, et al. (2017) The rapid evolution of highly efficient perovskite solar cells. *Energy Environ Sci* 10: 710–727. https://dx.doi.org/10.1039/C6EE03397K

11. Bouich A, Marí-Guaita J, Soucase BM, et al. (2023) Bright future by enhancing the stability of methylammonium lead triiodide perovskites thin films through Rb, Cs and Li as dopants. *Mater Res Bull* 163: 112213. https://dx.doi.org/10.1016/j.materresbull.2023.112213
12. Machín A, Márquez F (2024) Advancements in photovoltaic cell materials: Silicon, organic, and perovskite solar cells. *Materials* 17: 1165. https://dx.doi.org/10.3390/ma17051165
13. Li Y, Li Y, Zhang Q, et al. (2023) Electrical transport properties of TiO_2/$MAPbI_3$ and SnO_2/$MAPbI_3$ heterojunction interfaces under high pressure. *RSC Adv* 13: 3333–3340. https://dx.doi.org/10.1039/D2RA08143A
14. Ali N, Shehzad N, Uddin S, et al. (2021) A review on perovskite materials with solar cell prospective. *Int J Energy Res* 45: 19729–19745. https://dx.doi.org/10.1002/er.7067
15. Djeradi S, Dahame T, Fadla MA, et al. (2024) High-throughput ensemble-learning-driven band gap prediction of double perovskites solar cells absorber. *Mach Learn Knowl* 6: 435–447. https://doi.org/10.3390/make6010022
16. Courtier NE, Cave JM, Foster JM, et al. (2019) How transport layer properties affect perovskite solar cell performance: Insights from a coupled charge transport/ion migration model. *Energy Environ Sci* 12: 396–409. https://dx.doi.org/10.1039/C8EE01576G
17. Mahmood K, Sarwar S, Mehran MT (2017) Current status of electron transport layers in perovskite solar cells: Materials and properties. *RSC Adv* 7: 17044–17062. https://dx.doi.org/10.1039/C7RA00002B
18. Krishna BG, Ghosh DS, Tiwari S (2023) Hole and electron transport materials: A review on recent progress in organic charge transport materials for efficient, stable, and scalable perovskite solar cells. *Chem Inorg Mater* 1: 100026. https://dx.doi.org/10.1016/j.cinorg.2023.100026
19. Liu W, Hu S, Pascual J, et al. (2023) Tin halide perovskite solar cells with open-circuit voltages approaching the Shockley-Queisser limit. *ACS Appl Mater Interfaces* 15: 32487–32495. https://dx.doi.org/10.1021/acsami.3c06538
20. Khatoon S, Chakraborty V, Yadav SK, et al. (2023) Simulation study of $CsPbI_xBr_1$-x and $MAPbI_3$ heterojunction solar cell using SCAPS-1D. *Sol Energy* 254: 137–157. https://dx.doi.org/10.1016/j.solener.2023.02.059
21. Le TXH, Nguyen TV, Amadou Yacouba Z, et al. (2017) Correlation between degradation pathway and toxicity of acetaminophen and its by-products by using the electro-Fenton process in aqueous media. *Chemosphere* 172: 1–9. https://dx.doi.org/10.1016/j.chemosphere.2016.12.060
22. Bhattarai S, Hossain MK, Madan J, et al. (2024) Performance improvement of HTL-free perovskite solar cells with the graded approach by numerical simulation. *J Phys Chem Solids* 184: 111691. https://dx.doi.org/10.1016/j.jpcs.2023.111691
23. Mikroyannidis JA, Kabanakis AN, Sharma SS, et al. (2011) A simple and effective modification of PCBM for use as an electron acceptor in efficient bulk heterojunction solar cells. *Adv Funct Mater* 21: 746–755. https://dx.doi.org/10.1002/adfm.201001807
24. Ecker B, Nolasco JC, Pallarés J, et al. (2011) Degradation effects related to the hole transport layer in organic solar cells. *Adv Funct Mater* 21: 2705–2711. https://dx.doi.org/10.1002/adfm.201100429
25. Al Dmour H (2023) SCAPS numerical analysis of graphene oxide/TiO_2 bulk heterojunction solar cell sensitized by N719 ruthenium dye. *East Eur J Phys*: 555–561. https://dx.doi.org/10.26565/2312-4334-2023-3-65

26. Bulowski W, Szwanda A, Gawlińska-Nęcek K, et al. (2024) Optimization of the ETL titanium dioxide layer for inorganic perovskite solar cells. *J Mater Sci* 59: 7283–7298. https://dx.doi.org/10.1007/s10853-024-09581-w
27. Hussain I, Tran HP, Jaksik J, et al. (2018) Functional materials, device architecture, and flexibility of perovskite solar cell. *Emergent Mater* 1: 133–154. https://dx.doi.org/10.1007/s42247-018-0013-1
28. Yella A, Heiniger L-P, Gao P, et al. (2014) Nanocrystalline rutile electron extraction layer enables low-temperature solution processed perovskite photovoltaics with 13.7% efficiency. *Nano Lett* 14: 2591–2596. https://dx.doi.org/10.1021/nl500399m
29. Claudine U, Zhang P, Raza S, et al. (2025) Synergistically modified Ti_2C MXene with poly glycidyl methacrylate and poly(3,4-ethylene dioxythiophene): Poly(styrene sulfonate) conducting polymers for enhanced photocatalytic degradation of ionic and cationic dyes. *Colloids Surf A* 713: 136497. https://dx.doi.org/10.1016/j.colsurfa.2025.136497
30. Zhang P, Yang H, Zheng Q, et al. (2025) Next-generation solar energy: Progress, stability, and prospects of polymer-modified Perovskite solar cells; A review. *Int J Hydrogen Energy* 106: 1088–1113. https://dx.doi.org/10.1016/j.ijhydene.2025.01.280
31. Aldosari M, Sohrabpoor H, Gorji NE (2016) Optical modeling of graphene contacted CdTe solar cells. *Superlattice Microstruct* 92: 242–248. https://dx.doi.org/10.1016/j.spmi.2016.02.023
32. Znidi F, Morsy M, Nizam Uddin M (2024) Recent advances of graphene-based materials in planar perovskite solar cells. *Next Nanotechnol* 5: 100061. https://dx.doi.org/10.1016/j.nxnano.2024.100061
33. Altarawneh RM (2022) Facile fabrication of new sensing platforms decorated with quinalizarin and PtNi alloy nanoparticles for highly sensitive aluminum determination. *Microchem J* 182: 107944. https://dx.doi.org/10.1016/j.microc.2022.107944
34. Yadav S, Gupta SK, Negi CMS (2025) Graphene derivatives as efficient hole transport materials for lead-free double perovskite (Cs_2SnI_6) solar cells: a numerical study. *Optoelectron Lett* 21: 155–159. https://dx.doi.org/10.1007/s11801-025-4020-1
35. Qadoos A, Rashid M, Naeem MN, et al. (2025) Bandgap engineering in graphene oxide (GO) via integrating DFT calculations with atmospheric-pressure microplasma (AMP) treatment for optoelectronic applications. *Hybrid Adv* 8: 100353. https://dx.doi.org/10.1016/j.hybadv.2024.100353
36. de Lima AH, Tavares CT, da Cunha CCS, et al. (2020) Origin of optical bandgap fluctuations in graphene oxide. *Eur Phys J B* 93: 105. https://dx.doi.org/10.1140/epjb/e2020-100578-7
37. Al-Madanat O, AlSalka Y, Dillert R, et al. (2021) Photocatalytic H_2 production from naphthalene by various TiO_2 photocatalysts: Impact of Pt loading and formation of intermediates. *Catalysts* 11: 107. https://dx.doi.org/10.3390/catal11010107
38. AlSalka Y, Al-Madanat O, Hakki A (2023) TiO_2-based photocatalytic hydrogen production: How to transfer it to an applicable approach? *Appl Catal A Gen*, 662. https://dx.doi.org/10.1016/j.apcata.2023.119287
39. Curti M, Alsalka Y, Al-Madanat O, et al. (2023) Isotopic substitution to unravel the mechanisms of photocatalytic hydrogen production. *Photocatal Hydrogen Prod Sustainable Energy*, 35–61. https://dx.doi.org/10.1002/9783527835423.ch3

40. Ombaka LM, McGettrick JD, Oseghe EO, et al. (2022) Photocatalytic H_2 production and degradation of aqueous 2-chlorophenol over B/N-graphene-coated Cu^0/TiO_2: A DFT, experimental and mechanistic investigation. *J Environ Manage* 311: 114822. https://dx.doi.org/10.1016/j.jenvman.2022.114822
41. Mohamad Noh MF, Teh CH, Daik R, et al. (2018) The architecture of the electron transport layer for a perovskite solar cell. *J Mater Chem C* 6: 682–712. https://dx.doi.org/10.1039/C7TC04649A
42. Altarawneh RM (2025) Enhancing ethanol electrooxidation in acidic media using Pt nanoparticles supported on metal oxide-modified vulcan XC72 nanocomposites. *Langmuir* 41: 11101–11112. https://dx.doi.org/10.1021/acs.langmuir.5c00838
43. Latrous AR, Mahamdi R, Touafek N, et al. (2021) Performance enhancement in CZTS solar cells by SCAPS-1D. *Int J Thin Fil Sci Tec* 10: 75–81. https://doi.org/10.18576/IJTFST/100201
44. Rahaman M, Hasan M, Moinuddin RM, et al. (2024) Numerical optimization of lead-based and lead-free absorber materials for perovskite solar cell (PSC) architectures: A SCAPS-1D simulation. *AIP Adv*, 14. https://dx.doi.org/10.1063/5.0217486
45. Al-Dmour H (2024) SCAPS numerical analysis of graphene oxide/zirconium disulfide solar cells. *East Eur J Phys* 2: 445–449. https://dx.doi.org/10.26565/2312-4334-2024-2-58
46. Burgelman M, Nollet P, Degrave S (2000) Modelling polycrystalline semiconductor solar cells. *Thin Solid Films* 361–362: 527–532. https://dx.doi.org/10.1016/S0040-6090(99)00825-1
47. Rachidy C, Hartiti B, Touhtouh S, et al. (2023) Numerical modelling of the effect of $MAPI_3$ thin film on ITO/TiO_2/MEH-PPV/Au solar cell. *Matériaux Tech* 111: 507. https://doi.org/10.1051/mattech/2024003
48. Liang C, Huang Z, Su J, et al. (2024) Study on performance optimization of perovskite solar cells based on $MAPbI_3$. *Adv Theory Simul* 7: 2301015. https://dx.doi.org/10.1002/adts.202301015
49. Al-Dmour H (2021) Capacitance response of solar cells based on amorphous Titanium dioxide (A-TiO_2) semiconducting heterojunctions. *AIMS Mater Sci* 8: 261–270. https://dx.doi.org/10.3934/matersci.2021017
50. Du T, Xu W, Xu S, et al. (2020) Light-intensity and thickness dependent efficiency of planar perovskite solar cells: charge recombination versus extraction. *J Mater Chem C* 8: 12648–12655. https://dx.doi.org/10.1039/D0TC03390A
51. Al Dmour H, Al-Trawneh S, Al-Taweel S (2021) Synthesis, characterization, and performance of oligothiophene cyanoacrylic acid derivatives for solar cell applications. *IJAAS* 8: 6. https://dx.doi.org/10.21833/ijaas.2021.06.015
52. Rai N, Rai S, Singh PK, et al. (2020) Analysis of various ETL materials for an efficient perovskite solar cell by numerical simulation. *J Mater Sci Mater Electron* 31: 16269–16280. https://dx.doi.org/10.1007/s10854-020-04175-z
53. Miah MH, Khandaker MU, Rahman MB, et al. (2024) Band gap tuning of perovskite solar cells for enhancing the efficiency and stability: Issues and prospects. *RSC Adv* 14: 15876–15906. https://dx.doi.org/10.1039/D4RA01640H
54. Guo Z, Yuan M, Chen G, et al. (2024) Understanding defects in perovskite solar cells through computation: Current knowledge and future challenge. *Adv Sci* 11: 2305799. https://dx.doi.org/10.1002/advs.202305799
55. Jiang S, Liu M, Zhao D, et al. (2024) Doping strategies for inorganic lead-free halide perovskite solar cells: progress and challenges. *Phys Chem Chem Phys* 26: 4794–4811. https://dx.doi.org/10.1039/D3CP05444F

56. Park N-G, Zhu K (2020) Scalable fabrication and coating methods for perovskite solar cells and solar modules. *Nat Rev Mater* 5: 333–350. https://dx.doi.org/10.1038/s41578-019-0176-2
57. Tress W (2017) Perovskite solar cells on the way to their radiative efficiency limit—Insights into a success story of high open-circuit voltage and low recombination. *Adv Energy Mater* 7: 1602358. https://dx.doi.org/10.1002/aenm.201602358
58. Mehmood S, Xia Y, Qu F, et al. (2023) Investigating the performance of efficient and stable planer perovskite solar cell with an effective inorganic carrier transport layer using SCAPS-1D simulation. *Energies* 16: 7438. https://doi.org/10.3390/en16217438
59. Lee MM, Teuscher J, Miyasaka T, et al. (2012) Efficient hybrid solar cells based on meso-superstructured organometal halide perovskites. *Science* 338: 643–647. https://dx.doi.org/doi:10.1126/science.1228604
60. Schulz P, Edri E, Kirmayer S, et al. (2014) Interface energetics in organo-metal halide perovskite-based photovoltaic cells. *Energy Environ Sci* 7: 1377–1381. https://dx.doi.org/10.1039/C4EE00168K
61. Wang J, Zhou X, Ni J, et al. (2021) High-performance perovskite solar cell based on mesoporous TiO_2 electron transport layer enabled by composite treatment strategy. *J Mater Sci: Mater Electron* 32: 28417–28425. https://dx.doi.org/10.1007/s10854-021-07221-6
62. Usman A, Bovornratanaraks T (2024) Modeling and optimization of modified TiO2 with aluminum and magnesium as ETL in MAPbI3 perovskite solar cells: SCAPS 1D frameworks. *ACS Omega* 9: 39663–39672. https://dx.doi.org/10.1021/acsomega.4c04505

Appendix

Graphical abstract